IEEE Access
Multidisciplinary | Rapid Review | Open Access Journal

Received April 15, 2019, accepted May 13, 2019, date of publication May 16, 2019, date of current version May 30, 2019.

Digital Object Identifier 10.1109/ACCESS.2019.2917313

A Multi-Objective Optimal Torque Distribution Strategy for Four In-Wheel-Motor Drive Electric Vehicles

CHENG LIN[1,2], SHENG LIANG[1], JIAN CHEN[1], AND XIANG GAO[1]
[1]National Engineering Laboratory for Electric Vehicles, Beijing Institute of Technology, Beijing 100081, China
[2]Collaborative Innovation Center of Electric Vehicles in Beijing, Beijing Institute of Technology, Beijing 100081, China

Corresponding author: Jian Chen (chenjian2017@bit.edu.cn)

This work was supported in part by the Beijing Municipal Science and Technology Commission under Grant D171100007517001, and in part by the National Natural Science Foundation of China under Grant 51575044.

ABSTRACT Since four in-wheel-motor drive electric vehicles (4IDEVs) are overactuated systems, the torque distribution strategy is crucial for improving the system efficiency, lateral stability, and safety. Hence, this paper proposes a multiobjective optimal torque distribution strategy for 4IDEVs to improve the vehicle yaw stability performance and energy efficiency. First, a motor energy loss model is built to describe the motor power loss characteristics, and an energy efficiency control allocation (EECA) method over the NEDC is proposed to analyze the model accuracy. Then, a hybrid model predictive control (hMPC)-based nonlinear yaw stability controller is employed to calculate the reference yaw moment and the active steering angle. Finally, a multiobjective controller is designed to minimize the drivetrain power loss while ensuring the vehicle stability, in which the four wheels torques are allocated to track the reference yaw moment. The proposed strategy is evaluated on the dSPACE-based platform over the single lane change test and fishhook steering test. The results indicate that the suggested torque distribution strategy can improve the vehicle stability on different conditions and the energy consumption is significantly reduced compared to an electric stability control (ESC) method.

INDEX TERMS Electric vehicles, torque distribution strategy, hybrid model predictive control (hMPC), multi-objective control.

I. INTRODUCTION

In nearly decades, electric vehicles (EVs) have been considered as a solution of the global energy crisis and environmental problems [1]. The electric energy of EVs can be completely provided by renewable energy sources. Therefore, both of the non-renewable energy consumption and the exhaust emissions will be significantly reduced as the market share of EVs rises. As a result, EVs have attracted a great attention from researchers. The four in-wheel-motor drive electric vehicle (4IDEV) is one of the advanced architectures of EVs. Compared with other vehicles, e.g., conventional internal combustion engine vehicles (ICVs), hybrid electric vehicles (HEVs) and plug-in HEVs (PHEVs), the energy efficiency and the actuation flexibility of 4IDEVs are improved thanks to its special structure of drivetrain [2], [3]. What's more, the driving torque and the braking torque on each wheel can be controlled more precisely, so that the system performance can be improved by applying novel control methods [4], [5]. For example, the energy efficiency can be improved by energy-efficiency control allocation (EECA) algorithms, the lateral stability can be enhanced by electric stability control (ESC) based on coordinated control of driving motors. On the other hand, the 4IDEV is a typical overactuated system, so the control system has a great impact on the system performance. However, the control problem of 4IDEVs is more complicated due to its nonlinear dynamic characteristics and strong system coupling [6].

On the Basis of actuation flexibility, lateral stability control for 4IDEVs have been greatly developed. According to different actuators, previous studies mostly focused on following two control methods:

1) Direct yaw moment control (DYC).

The actuators of DYC are independent drive motors equipped on 4IDEVs. In a DYC process, the vehicle lateral

The associate editor coordinating the review of this manuscript and approving it for publication was Xu Chen.

stability can be controlled by a yaw moment which is generated by the torque distribution strategy [7].

2) Active steering system (AS) control:

In AS control, the actuator is an electric motor which is used to generate the active steering torque. The active steering torque is calculated by the control module of AS for lateral stability enhancement [8].

Various studies on DYC for 4IDEVs have been discussed in literature. Sakai *et al.* [7] proposed a dynamic driving/braking force distribution algorithm to equalize loads on wheels for vehicle stability improvement. Chen and Kuo [9] proposed a DYC strategy for EVs with four in-wheel motors which consists of three hierarchical controllers to achieve better handling performance. Choi and Choi [10] presented an optimal braking forces allocation method based on model predictive control (MPC), which used the bicycle model with lagged tire force to achieve better control performance. De Novellis *et al.* [11] proposed a wheel torque distribution criteria with torque-vectoring differentials and compared the control performance between proposed method and an energy-based torque distribution method. Zhai *et al.* [12] designed a hierarchical DYC-based ESC algorithm for an EV equipped with four in-wheel motors and a stability judgment controller is proposed to switch proper control modes. Liu *et al.* [13] presented a hierarchical control strategy for a hybrid electric ground vehicle (HEGV) driven by eight in-wheel motors.

On the other hand, the AS-based methods have also gotten certain attention. Falcone *et al.* [8] presented a MPC approach for an active front steering (AFS) system in an autonomous vehicle to improve the lateral stability. Nam *et al.* [14] proposed a robust yaw stability control based on AS control considered the model uncertainty. A μ control based strategy for a four-wheel steer-by wire vehicle was designed by Zhao *et al.* [15], the lateral stability control performance and steering flexibility were improved by calculating the optimal front and rear steering angles simultaneously.

Furthermore, some researchers have proposed integrated control strategies that combine DYC and AS. Di Cairano *et al.* [16] proposed a hybrid model predictive control (hMPC) strategy of AFS and DYC based on the bicycle model with a tire brush model. Zhao *et al.* [17] designed a triple-step nonlinear integrated control scheme with AFS and DYC for 4IDEVs. Ren *et al.* [18] proposed a MPC controller of AFS and DYC and a holistic control structure is built to simplify the control system. Xie *et al.* [19] proposed an integrated control system that includes DYC and rear-wheel-active-steering (RAS) system to ensure vehicle stability for a four-wheel steering 4IDEV. Guo *et al.* [20] proposed a novel hierarchical controller includes an adaptive sliding mode high-level algorithm and a pseudo-inverse control allocation strategy for four-wheel independent drive autonomous vehicles and the immeasurable disturbances are estimated by a fuzzy control system.

The energy efficiency optimization for 4IDEVs is another research hotspot. Chen and Wang [21], [22] presented a fast Karush-Kuhn-Tucker (KKT)-based algorithm for an energy-efficient control allocation (EECA) scheme and compared the proposed KKT-based EECA with an adaptive EECA and a simple rule-based EECA. The EECA method proposed by Yuan and Wang [23] focused on high speed and low torque regions of motors and presented an optimized torque distribution strategy for energy-efficiency improving. Dizquh *et al.* [24] proposed a fast and parametric torque distribution strategy for 4IDEVs by setting the optimal switch point between the even torque distribution and the single-axle drive strategy. Wang *et al.* [25] proposed a real-time torque distribution strategy and combined it with a particle swarm optimization-based component sizing. The performance of previous studies are mostly analyzed over the New European Driving Cycle (NEDC).

Additionally, multi-objective optimization methods considered both lateral stability and energy efficiency have been presented in recent years. Prior researches suggest that the multi-objective optimization controller can further improve the system performance in complicated conditions in practice. He *et al.* [26] proposed a quadratic programing (QP)-based optimal torque distribution strategy to minimize the power loss of drivetrain and improve the lateral stability by utilizing the tire-road friction of each wheel. In [27], a multi-objective optimization method was proposed based on non-convex optimization with the penalty function consisting of the yaw moment control offset, the drive system energy loss and the slip ratio constraint. Jing *et al.* [28] presented a multi-objective optimal control allocation strategy to trade off energy efficiency and lateral stability by combining the EECA and a MPC-based allocation.

In this paper, the proposed hierarchical torque distribution strategy for 4IDEVs is based on multi-objective optimization. An energy loss model of 4IDEV is proposed in section II and an EECA strategy based on the proposed model is presented and analyzed over the NEDC. A hMPC-based yaw stability controller which combines DYC and AS is described in section III for lateral stability enhancement and the nonlinear characteristics of lateral tire forces are simplified by a piecewise linear approximation. In section IV, a multi-objective torque distribution controller considering both of the energy efficiency and lateral stability is presented. The simulation results of the proposed control strategy are demonstrated on the dSPACE-based platform in Section V, followed by conclusions presented in section VI. The proposed multi-objective control system schematic is shown in Fig. 1.

II. ENERGY LOSS MODEL

A. MOTOR ENERGY LOSS MODEL

The motor energy loss is the largest part of total energy loss, so it is important to build an energy loss model to describe the characteristics of it. The efficiency MAP of motors based on the experimental results is shown in Fig. 2. The measurement interval of torque is 10 N·m and the measurement interval of motor speed is 800 rev/min.

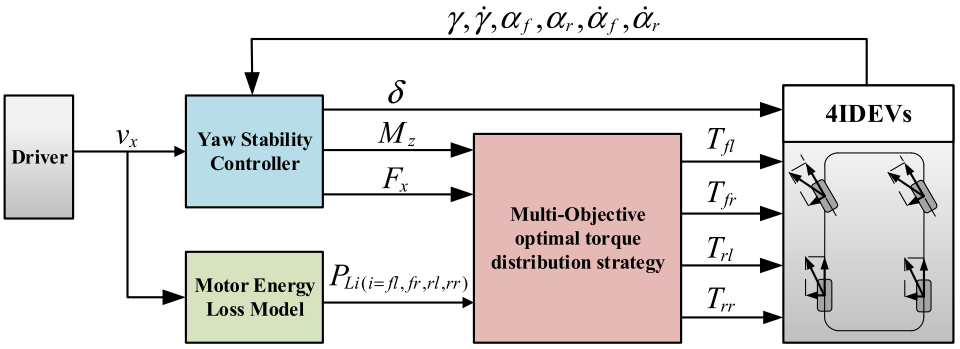

FIGURE 1. Multi-objective control system structure.

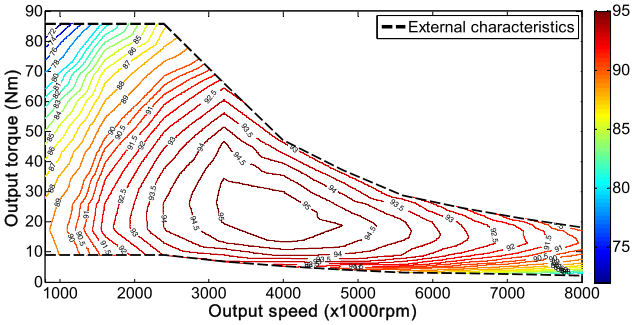

FIGURE 2. Efficiency MAP of motors.

To describe the motor efficiency characteristics properly, the motor power loss varies with torque at different motor speeds is fitted by polynomial functions. A fitting order estimation method based on leave-one-out cross-validation (LOOCV) is proposed in this section to ensure the fitting accuracy and prevent overfitting. In this paper, experimental data of power loss at a certain speed is fitted with polynomial functions up to 4th-order and the most accurate fitting order is selected by LOOCV. In each order, the data is fitted for 10000 times and a data point is left randomly at each time. The fitting results is compared with experimental data and the average LOOCV error is expressed in

$$e_k = \frac{1}{10000}\sum_{i=1}^{10000}\left[\sum_{j=1}^{S}\left(y_j - \hat{y}_j\right)^2\right] \tag{1}$$

where e_k is the error of k-th approximation, i and j are the number of fitting times and data points, S is the amount of data, y_n and $\hat{y}_n$ are the values of experiment data and the corresponding fitting results. The average LOOCV errors and the proper fitting order is shown in Table 1.

The fitting results show that power loss functions from 800 rev/min to 8000 rev/min are non-convex at low torque region and convex at high torque region. Fig. 3 shows the 3rd-order approximation at 800 rev/min and the 4th-order approximation at 2400 rev/min. It is obvious that the concavity is certain at both cases.

TABLE 1. LOOCV results.

Speed (rpm)	e_1	e_2	e_3	e_4	Fitting order
800	0.2786	0.0693	0.0143	0.0502	3
1600	0.2606	0.0566	0.0054	0.0092	3
2400	0.1869	0.0217	0.0040	0.0022	4
3200	0.0333	0.0094	0.0007	0.0006	4
4000	0.0230	0.0079	0.0024	0.0010	4
4800	0.0150	0.0075	0.0040	0.0028	4
5600	0.0106	0.0100	0.0026	0.0068	3
6400	0.0807	0.0138	0.0055	0.0075	3
7200	0.1290	0.0029	0.0108	0.0231	3
8000	0.2290	0.0476	0.0245	0.0303	3

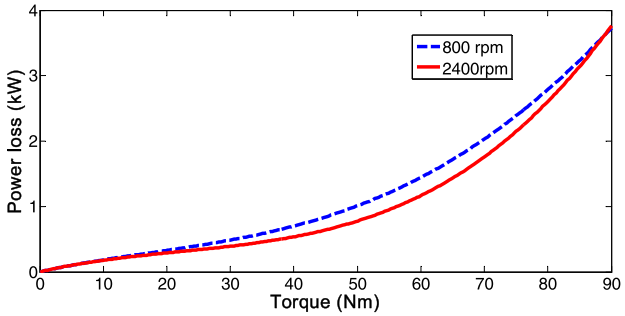

FIGURE 3. Power loss function at 800 rev/min and 2400 rev/min.

B. EECA STRATEGY OVER THE NEDC

On the basis of the proposed energy loss model, an EECA strategy is proposed over the NEDC. In this section, the lateral motion is neglected. Therefore, the EECA problem can be simplified to a torque distribution problem for a half-car model.

The objective of EECA strategy is minimizing the power loss of drivetrain. The cost function of the proposed EECA strategy consists of two terms, the first term is the power loss of front motors and the second is the power loss of rear motors. Hence, the EECA problem is formulated as follows:

$$\begin{aligned} &\min J_P = \min[P_L(T_f, n) + P_L(T_r, n)] \\ &\text{subj.to. } n = \frac{v_{NEDC}\cdot i_0}{r} \\ &\qquad T_f + T_r = \frac{T_{NEDC}}{2} \end{aligned} \tag{2}$$

where J_P is the cost function, T_f and T_r are torques of motors equipped on front axle and rear axle, n is motor speed, $P_L(T, n)$ is the power loss function varies with torque and motor speed. The power loss function can be expressed in $P_L(T)$ if the motor speed is constant. i_0 and r are the transmission ratio and tire rolling radius. v_{NEDC} and T_{NEDC} are required vehicle velocity and required torque of all motors determined by the NEDC. Fig. 4 shows v_{NEDC} and absolute values of T_{NEDC}.

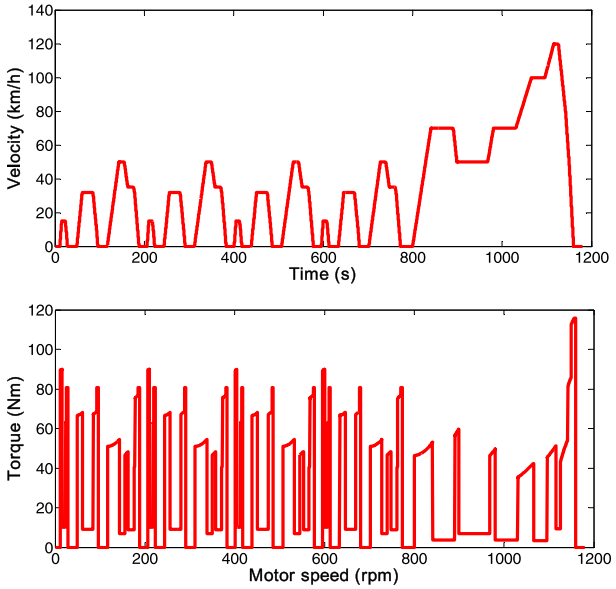

FIGURE 4. Required vehicle velocity and absolute values of required torque.

An equivalent form of the definition of convex functions shows that the following equation is always true if $f(x)$ is a convex function:

$$f\left(\frac{x_1+x_2}{2}\right) \le \frac{f(x_1)+f(x_2)}{2} \tag{3}$$

where x_1 and x_2 are any two values at the domain of $f(x)$.

According to (3), suppose $x_1 = 0$ and $x_2 = T_{NEDC}/2$, the single axle driving strategy has the optimal energy efficiency if the half required torque is in the non-convex region.

On the other hand, the optimal distribution strategy cannot be determined directly by the concavity. Suppose $P_L(T)$ is a k-th polynomial function. Therefore, the Taylor series of power loss functions around $T^* = (T_f + T_r)/2$ is expressed in

$$\begin{aligned} P_L(T) \approx\ & P_L(T^*)+P'_L(T^*)(T^*-T) \\ & +\frac{1}{2}P''_L(T^*)(T^*-T)^2+\frac{1}{3!}P^{(3)}_L(T^*)(T^*-T)^3 \\ & +\frac{1}{4!}P^{(4)}_L(T^*)(T^*-T)^4+\ldots+\frac{1}{\mathrm{k}!}P^{(\mathrm{k})}_L(T^*)(T^*-T)^k \end{aligned} \tag{4}$$

Then the Taylor series of J_P can be expressed in:

$$\begin{aligned} J_p =\ & P_L(T_f)+P_L(T_r) \\ \approx\ & [P_L(T^*)+P'_L(T^*)(T^*-T_f) \\ & +\frac{1}{2}P''_L(T^*)(T^*-T_f)^2+\frac{1}{3!}P^{(3)}_L(T^*)(T^*-T_f)^3 \\ & +\frac{1}{4!}P^{(4)}_L(T^*)(T^*-T_f)^4+\ldots+\frac{1}{\mathrm{k}!}P^{(\mathrm{k})}_L(T^*)(T^*-T_f)^k] \\ & +[P_L(T^*)+P'_L(T^*)(T^*-T_r) \\ & +\frac{1}{2}P''_L(T^*)(T^*-T_r)^2+\frac{1}{3!}P^{(3)}_L(T^*)(T^*-T_r)^3 \\ & +\frac{1}{4!}P^{(4)}_L(T^*)(T^*-T_r)^4+\ldots+\frac{1}{\mathrm{k}!}P^{(\mathrm{k})}_L(T^*)(T^*-T_r)^k] \end{aligned} \tag{5}$$

According to the constrains in (2), the T_f and T_r can be expressed in

$$\begin{aligned} T_f &= T^* + \Delta T \\ T_r &= T^* - \Delta T \end{aligned} \tag{6}$$

where ΔT is an amount around T^*. By substituting (6) into (5), J_P is simplified as follows:

$$\begin{aligned} J_p \approx\ & 2\cdot P_L(T^*)+P''_L(T^*)\cdot\Delta T^2+\frac{2}{4!}P^{(4)}_L(T^*)\cdot\Delta T^4 \\ & +\ldots+\frac{2}{k^*!}P^{(k^*)}_L(T^*)\cdot\Delta T^{\mathrm{k}^*} \end{aligned} \tag{7}$$

where k^* is the largest even number smaller than k. On the basis of the proposed motor energy loss model, $k^* = 2$ if $P_L(T)$ is a 3rd-order polynomial function and $k^* = 4$ if $P_L(T)$ is a 4th-order polynomial function. As a result, in the first case, $P_L(T)$ is monotonically increasing about ΔT if $P''_L(T^*)$ is positive and vice versa. On the other hand, in the second case, $P_L(T)$ is monotonically increasing about ΔT if $P''_L(T^*) \ge -12P^{(4)}_L(T^*)\cdot\max(\Delta T)^2$ and vice versa. Here the EECA problem is simplified into finding a switching point between even distribution and single axle driving.

Suppose $\max(\Delta T)$ equals to T^*, the optimal solution of (2) at a certain motor speed can be summarized as follows:

1) If $P_L(T)$ is a 3rd-order polynomial function, the switching point is inflection point of $P_L(T)$.

2) If $P_L(T)$ is a 4th-order polynomial function, the switching condition is $P''_L(T^*) \ge -12P^{(4)}_L(T^*)\cdot T^{*2}$.

The switching points are determined offline. The function of switching points varies motor torque is shown in Fig. 5.

The proposed optimal EECA strategy is analyzed over the NEDC. Fig. 6 compares the power loss of the optimal EECA strategy and even distribution strategy. The simulation result in Table 2 shows that the total energy loss can be reduced by 9.29% with the optimal EECA strategy.

III. YAW STABILITY CONTROLLER

The vehicle yaw stability control system [29] is able to reduce the deviation between the driver's intention and the actual vehicle motion under adverse driving conditions. Since the

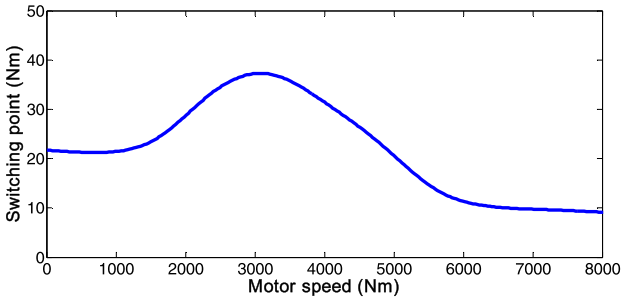

FIGURE 5. The function of switching points.

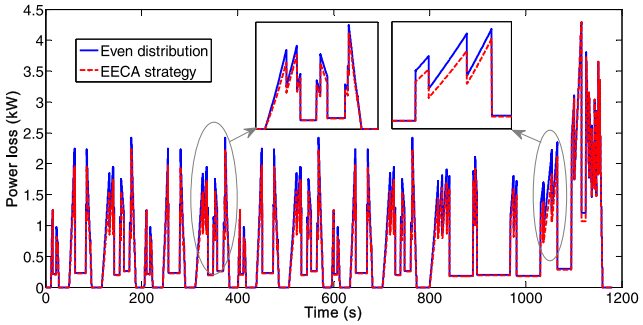

FIGURE 6. Power loss over the NEDC.

TABLE 2. Power loss comparison over the NEDC cycle.

	Optimal EECA strategy (kW)	Even distribution (kW)	EECA improvement (%)
Power loss	64566.4	71178.6	9.29%

independent and continuous wheel torque control is the distinct characteristic of 4IDEVs, the vehicle lateral stability and handing performance can be ameliorated by DYC and AS. In this section, a hMPC-based yaw stability controller is designed to track the desired states and stabilize the vehicle quickly. For the further application in the following torque distribution, the hMPC controller is built to calculate the value of the desired yaw moment and steering angle when the vehicle is unstable.

A. VEHICLE DYNAMIC MODEL

To stabilize the vehicle with the hMPC controller, a mixed logical dynamical (MLD) model [30] is required to predict the future vehicle behavior. The MLD model can be formulated from a hybrid nonlinear vehicle dynamic model, which mainly consists of a 2 DOF vehicle model and a piecewise linear tire model.

1) TIRE MODEL

Vehicle dynamics control is achieved by directly or indirectly adjusting contact forces between tires and the ground. The nonlinear characteristics of the tires and the complex changes in the contact area between the elastic tire and the ground have a profound impact on the steering characteristics and driving stability of the vehicle. Therefore, the dynamic simulation of the vehicle requires an accurate tire model.

In this paper, the tire model is developed based on the magic tire model. Ignoring the horizontal shift S_{hi} and vertical shift S_{vi}, the tire lateral forces F_{yi} is related to the tire sideslip angle α_i and normal vertical force under the pure steering condition as follows:

$$F_{yi} = D_{yi}\sin\{C_{yi}\arctan[B_{yi}\alpha_i - E_{yi}(B_{yi}\alpha_i - \arctan B_{yi}\alpha_i)]\} \quad (8)$$

where the subscript $i \in \{f, r\}$ represents the front or rear tires, B_{yi}, C_{yi}, D_{yi} and E_{yi} are stiffness factor, shape factor, peak factor and curvature factor, respectively, which depend on the normal vertical force and α_i.

However, the complicated magic tire model with high nonlinearity is detrimental to the calculation speed of the yaw stability controller. Considering the nonlinear characteristic of tires, we can approximate the magic tire model with a piecewise linear function. With the assumption that there is no wheel sliding or slipping, we can obtain the fitting function as follows:

$$F_{yi} = \begin{cases} k_{2i}\alpha_i - m_{2i} & \text{if } \alpha_i \in (-\infty, -f_{bi}) \\ k_{1i}\alpha_i - m_{1i} & \text{if } \alpha_i \in [-f_{bi}, -f_{ai}) \\ c_i\alpha_i & \text{if } \alpha_i \in [-f_{ai}, f_{ai}] \\ k_{1i}\alpha_i + m_{1i} & \text{if } \alpha_i \in (f_{ai}, f_{bi}] \\ k_{2i}\alpha_i + m_{2i} & \text{if } \alpha_i \in (f_{bi}, +\infty) \end{cases} \quad (9)$$

where c_i is the tire cornering stiffness, k_{1i}, m_{1i}, k_{2i} and m_{2i} are the fitting coefficients, f_{ai} and f_{bi} are the segregating points.

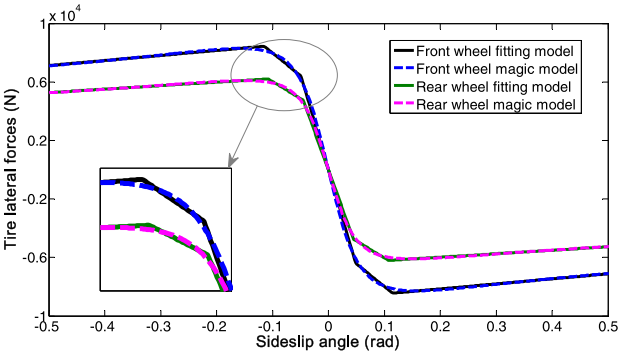

FIGURE 7. Lateral tire forces of front and rear tires.

As shown in Fig. 7, the continuous lateral tire model is divided into five discrete regions, and the regions are switched by the value of α_i. Fig. 7 illustrates that the fitting error between the piecewise linear curve and magic model is quite small. Hence, the proposed tire model is practicable in the following vehicle model.

2) VEHICLE MODEL

A 2 DOF bicycle model is chosen as the vehicle model for the yaw stability control. As shown in Fig. 8, in this model, the

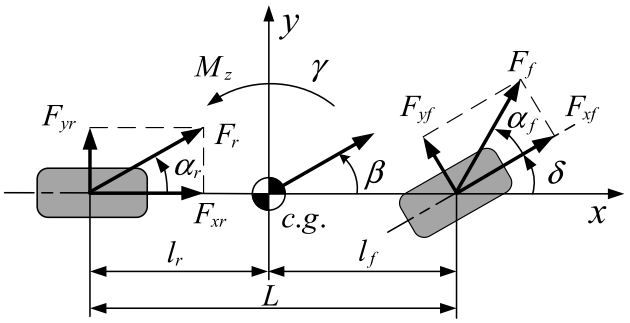

FIGURE 8. 2 DOF bicycle model.

distance between the wheels of front and rear axles is ignored and the pitch and roll motion of the vehicle is not considered. In addition, the longitudinal velocity v_x is assumed to be constant in this paper. Hence, the longitudinal traction formula can be further neglected. The x, y axis in Fig. 8 is attached to the vehicle center of mass and moves with the vehicle. The lateral and yaw motion of the vehicle can be described respectively in following equations:

$$mv_x\left(\dot{\beta}+\gamma\right) = F_{yf}+F_{yr} \tag{10}$$

$$I_z\dot{\gamma} = l_fF_{yf}-l_rF_{yr}+M_z \tag{11}$$

where β, γ, I_z and M_z represent the vehicle sideslip angle, vehicle yaw rate, vehicle inertia along the z axis and yaw moment, respectively, l_f and l_r are the longitudinal distance from the c.g. to front or rear axle.

Since the tire slip angles and steering angle δ are rather small in general, the tire slip angles can be approximated as follows:

$$\alpha_f = \beta-\delta+\frac{l_f\gamma}{v_x} \tag{12}$$

$$\alpha_r = \beta-\frac{l_r\gamma}{v_x} \tag{13}$$

Hence, the yaw rate γ can be expressed as follows:

$$\gamma = \frac{v_x}{L}(\alpha_f-\alpha_r+\delta) \tag{14}$$

where $L = l_f + l_r$ is the longitudinal distance from the front axle to rear axle.

Plugging (10), (11) and (14) into (12) and (13), we can obtain:

$$\begin{aligned}\dot{\alpha}_f = {} & \frac{1}{mv_x}(F_{yf}+F_{yr})-\frac{v_x}{L}(\alpha_f-\alpha_r+\delta_f)\\ & +\frac{l_f}{v_xI_z}(l_fF_{yf}-l_rF_{yr}+M_z)-\dot{\delta}\end{aligned} \tag{15}$$

$$\begin{aligned}\dot{\alpha}_r = {} & \frac{1}{mv_x}(F_{yf}+F_{yr})-\frac{v_x}{L}(\alpha_f-\alpha_r+\delta_f)\\ & -\frac{l_r}{v_xI_z}(l_fF_{yf}-l_rF_{yr}+M_z)\end{aligned} \tag{16}$$

Ignoring the minus effect of the steering angle on the vehicle dynamics, (14), (15) and (16) can be rewritten as the following state-space representation:

$$\begin{aligned}\dot{\boldsymbol{x}} &= \boldsymbol{A_{pq}x}+\boldsymbol{B_{pq}u}+\boldsymbol{f_{pq}}\\ \boldsymbol{y} &= \boldsymbol{C_{pq}x}+\boldsymbol{D_{pq}u}\\ &\text{if } \boldsymbol{x}\in\boldsymbol{\chi_{pq}}\end{aligned} \tag{17}$$

where the vehicle state $\boldsymbol{x} = [\alpha_f\alpha_r]^T$, control variable $\boldsymbol{u} = [\delta M_z]^T$ and system output $\boldsymbol{y} = \gamma$. The matrices $\boldsymbol{A_{pq}}, \boldsymbol{B_{pq}}, \boldsymbol{C_{pq}}$ and $\boldsymbol{f_{pq}}$, $p, q \in \{1, \ldots, 5\}$ define the vehicle dynamics when the tire sideslip angles of the front and rear wheels are in the p-th and q-th regions in (9), i.e., $\boldsymbol{\chi_{pq}}$, respectively.

The control objective of the yaw stability controller is to force the output γ to track the reference signal γ_d quickly and precisely. To minimize the tracking error during the control process, the extended state $\boldsymbol{x}_e = [\alpha_f\alpha_rE_s\gamma_d]^T$ is defined, where E_s is the accumulative tracking error of yaw rate as follows:

$$E_{s(k+1)} = E_{s(k)}+\gamma_{(k)}-\gamma_{d(k)} \tag{18}$$

$$\gamma_{d(k+1)} = \gamma_{d(k)} \tag{19}$$

where k represents the k-th sampling time.

Thereby, (17) can be formulated to an extended closed-loop discrete-time system as below:

$$\begin{aligned}\boldsymbol{x}_{e(k+1)} &= \boldsymbol{A^*_{pq}x}_{e(k)}+\boldsymbol{B^*_{pq}u}_{(k)}+\boldsymbol{f^*_{pq}}\\ \boldsymbol{y}_{(k)} &= \boldsymbol{C^*_{pq}x}_{e(k)}+\boldsymbol{D^*_{pq}u}_{(k)}\\ &\text{if } \boldsymbol{x}_{e(k)}\in\boldsymbol{\chi}_{epq(k)}\end{aligned} \tag{20}$$

where the matrices $\boldsymbol{A^*_{pq}}$, $\boldsymbol{B^*_{pq}}$, $\boldsymbol{C^*_{pq}}$, $\boldsymbol{D^*_{pq}}$ and $\boldsymbol{f^*_{pq}}$ are the discretized corresponding matrices in (17).

Since there are five regions of the front and rear tire lateral force, respectively, the discrete-time hybrid vehicle model described in (20) have 25 modes in total, and the active mode is switched depending on the range of the states and the region of linearity. For the further application in the hMPC controller, (20) need to be transformed to a MLD model form, which is described by interdependent physical laws, logic rules, and operating constraints. The construction of a MLD model can be achieved by using the hybrid system description language (HYSDEL) [31].

To deal with the switching points between different regions of (20), a binary variable $\boldsymbol{v} \in \{0, 1\}^m$ is defined. Thus the discrete-time system can be expressed as follows:

$$\begin{aligned}\boldsymbol{x}_{e(k+1)} &= \boldsymbol{A}\boldsymbol{x}_{e(k)}+\boldsymbol{B}_1\boldsymbol{u}_{(k)}+\boldsymbol{B}_2\boldsymbol{v}_{(k)}+f(\boldsymbol{x}_{e(k)},\boldsymbol{v}_{(k)})\\ \boldsymbol{y}_{(k)} &= \boldsymbol{C}\boldsymbol{x}_{e(k)}+\boldsymbol{D}_1\boldsymbol{u}_{(k)}+\boldsymbol{D}_2\boldsymbol{v}_{(k)}+g(\boldsymbol{x}_{e(k)},\boldsymbol{v}_{(k)})\end{aligned} \tag{21}$$

where $f(\boldsymbol{x}_{e(k)}, \boldsymbol{v}_{(k)})$ and $g(\boldsymbol{x}_{e(k)}, \boldsymbol{v}_{(k)})$ are the nonlinear functions of $\boldsymbol{x}_{e(k)}$ and $\boldsymbol{v}_{(k)}$. Hence, the regions of (20) can be determined by the values of $\boldsymbol{v}_{(k)}$.

In addition, $f(\boldsymbol{x}_{e(k)}, \boldsymbol{v}_{(k)})$ and $g(\boldsymbol{x}_{e(k)}, \boldsymbol{v}_{(k)})$ can be further simplified by defining a new variable $\boldsymbol{z}_{(k)}$ and the additional constrains of $\boldsymbol{v}_{(k)}$ and $\boldsymbol{z}_{(k)}$ [30]. Thereby, (21) can be translated to a MLD model and expressed as follows:

$$\begin{aligned}\boldsymbol{x}_{e(k+1)} &= \boldsymbol{A}\boldsymbol{x}_{e(k)}+\boldsymbol{B}_1\boldsymbol{u}_{(k)}+\boldsymbol{B}_2\boldsymbol{v}_{(k)}+\boldsymbol{B}_3\boldsymbol{z}_{(k)}\\ \boldsymbol{y}_{(k)} &= \boldsymbol{C}\boldsymbol{x}_{e(k)}+\boldsymbol{D}_1\boldsymbol{u}_{(k)}+\boldsymbol{D}_2\boldsymbol{v}_{(k)}+\boldsymbol{D}_3\boldsymbol{z}_{(k)}\\ \boldsymbol{E}_1\boldsymbol{v}_{(k)}+\boldsymbol{E}_2\boldsymbol{z}_{(k)} &\le \boldsymbol{E}_3\boldsymbol{x}_{e(k)}+\boldsymbol{E}_4\boldsymbol{u}_{(k)}+\boldsymbol{E}_5\end{aligned} \tag{22}$$

where $\boldsymbol{A}, \boldsymbol{B}_1, \boldsymbol{B}_2, \boldsymbol{B}_3, \boldsymbol{C}, \boldsymbol{D}_1, \boldsymbol{D}_2, \boldsymbol{D}_3$ and $\boldsymbol{E}_1, \ldots, \boldsymbol{E}_5$ are matrices of suitable dimensions determined by HYSDEL [31].

B. HMPC CONTROLLER DESIGN

On the basis of the MPC theory in [32], at each sample time, the current system state is set as the initial state of the optimal control problem, and the current control action is determined by solving the optimal control problem in the further P sampling periods. Only the first optimal input is applied on the system in the optimal input sequence of length N. P and N are identified as the prediction horizon and control horizon, respectively. Meanwhile, the output is approaching the reference value in the receding horizon control process.

The predictive model of a hMPC controller is a hybrid system described in (20). Besides the general continuous variables, the integer variables are used to select the system mode in the MLD model. The object of the hMPC controller is to obtain the desired yaw moment M_{zd} and the steering angle δ by tracking the reference value of yaw rate γ_d under constrains.

1) REFERENCE AND CONSTRAINTS

The reference value of yaw rate for the vehicle yaw stability control is usually calculated on the basis of a linear 2 DOF bicycle model in which the lateral front and rear tire forces are linear as follows:

$$F_{yf} = c_f \alpha_f \tag{23}$$
$$F_{yr} = c_r \alpha_r \tag{24}$$

By plugging (12), (13), (23) and (24) into (10) and (11), the reference value of yaw rate γ_d can be calculated by the transfer function from steering angle to yaw rate as follow:

$$\gamma_d(s) = \frac{\frac{c_f l_f}{I_z} s + \frac{c_f^2 L}{m v_x I_z}}{s^2 + (\frac{c_f l_f^2 + 2c_r l_r^2}{v_x I_z} + \frac{c_f + 2c_r}{m v_x}) s + \frac{c_f c_r L^2 - m v_x^2 (c_f l_f - c_r l_r)}{m v_x^2 I_z}} \delta(s) \tag{25}$$

In addition, some constraints should be taken into account. To ensure that the vehicle remains stable, the states should be limited in a certain range. To make the states vector stay in the convergence region of system, the constraints of states can be described as follows:

$$\begin{aligned} \alpha_{f\,\min} \le \alpha_f \le \alpha_{f\,\max} \\ \alpha_{r\,\min} \le \alpha_r \le \alpha_{r\,\max} \end{aligned} \tag{26}$$

Moreover, considering some physical constraints on 4IDEVs, such as the restriction of the capability of the drive motors and the steering space, the constraints of the inputs are defined as follows:

$$\begin{aligned} \delta_{\min} \le \delta_{(k+i|k)} \le \delta_{\max} \\ M_{z\min} \le M_{z(k+i|k)} \le M_{z\max} \end{aligned} \tag{27}$$

2) OPTIMATION OBJECTIVE

The cost function of the hMPC controller is to stabilize the 4IDEV effectively, i.e., keep the yaw rate as close as possible to its reference value γ_d with the control of the optimal input sequence of δ and M_{zd}. Hence, the cost function is defined as the sum of the 2-norm case of the matrix which reflects the distance between the outputs and their corresponding reference values. Due to the hybrid MPC algorithm, the whole control problem can be divided into receding horizon control problems. The receding horizon control problem at the k-th sampling time is shown in the follow:

$$\begin{aligned} &\min J_k = \min_{k \to k+N-1} \|\boldsymbol{Y_k} - \boldsymbol{R_k}\|_{\boldsymbol{Q}}^2 \\ &= \min \sum_{i=0}^{N-1} (\boldsymbol{y_{k+i|k}} - \boldsymbol{r_{k+i|k}})^T \boldsymbol{Q} (\boldsymbol{y_{k+i|k}} - \boldsymbol{r_{k+i|k}}) \\ &\text{subj.to. } \boldsymbol{x_{e(k+1)}} = \boldsymbol{A x_{e(k)}} + \boldsymbol{B}_1 \boldsymbol{u_{(k)}} + \boldsymbol{B}_2 \boldsymbol{v_{(k)}} + \boldsymbol{B}_3 \boldsymbol{z_{(k)}} \\ &\qquad \boldsymbol{y_{(k)}} = \boldsymbol{C x_{e(k)}} + \boldsymbol{D}_1 \boldsymbol{u_{(k)}} + \boldsymbol{D}_2 \boldsymbol{v_{(k)}} + \boldsymbol{D}_3 \boldsymbol{z_{(k)}} \\ &\qquad \boldsymbol{E}_1 \boldsymbol{v_{(k)}} + \boldsymbol{E}_2 \boldsymbol{z_{(k)}} \le \boldsymbol{E}_3 \boldsymbol{x_{e(k)}} + \boldsymbol{E}_4 \boldsymbol{u_{(k)}} + \boldsymbol{E}_5 \\ &\qquad \boldsymbol{u_{(k+i|k)}} \in \boldsymbol{U_k}, \boldsymbol{x_{e(k|k)}} = \boldsymbol{x_{e(k)}}, \boldsymbol{x_{e(k+N|k)}} \in \boldsymbol{\chi_f} \\ &\qquad \alpha_{f\,\min} \le \alpha_{f(k+i|k)} \le \alpha_{f\,\max} \\ &\qquad \alpha_{r\,\min} \le \alpha_{r(k+i|k)} \le \alpha_{r\,\max} \\ &\qquad \delta_{\min} \le \delta_{(k+i|k)} \le \delta_{\max} \\ &\qquad M_{z\min} \le M_{z(k+i|k)} \le M_{z\max} \end{aligned} \tag{28}$$

where $\boldsymbol{U_k} = \begin{bmatrix} \boldsymbol{u_{k|k}} \\ \boldsymbol{u_{k+1|k}} \\ \cdot \\ \cdot \\ \boldsymbol{u_{k+N-1|k}} \end{bmatrix}_N \subseteq \mathbb{R}^N$, $\boldsymbol{Y_k} = \begin{bmatrix} \boldsymbol{y_{k|k}} \\ \boldsymbol{y_{k+1|k}} \\ \cdot \\ \cdot \\ \boldsymbol{y_{k+P-1|k}} \end{bmatrix}_P \in R^P$ and $\boldsymbol{R_k} = \begin{bmatrix} \boldsymbol{r_{k|k}} \\ \boldsymbol{r_{k+1|k}} \\ \cdot \\ \cdot \\ \boldsymbol{r_{k+N-1|k}} \end{bmatrix}_P \in \mathbb{R}^P$ are the control sequence, output sequence and output reference sequence, respectively. $\boldsymbol{x_{e(k)}}$ is the state at the k-th sampling time, $\boldsymbol{\chi_f}$ is the controller terminal set. $\boldsymbol{Q}$ is the weight matrix of output. As $\boldsymbol{Q}$ increases, the control effect of the output will increase, i.e., the optimized value will reduce.

Considering the logical variables in the constraints defined in the MLD model, the predictive control problem with constraints has no optimal solution in analytic form. Since the problem described in (28) contains both integer and continuous variables, the tracking problem is termed a mixed integer programming (MIP). In virtue of the norm in the objective function (28) is squared Euclidean norm, the problem further comes down to solve a mixed integer quadratic programming (MIQP) via the ILOG CPLEX solver. The optimal yaw moment and steering angle can be obtained by solving the MIQP problem.

IV. MULTI-OBJECTIVE TORQUE DISTRIBUTION CONTROLLER

To determine the optimal torque distribution for 4IDEV, a torque distribution controller should be built to calculate the driving torques or braking torques of four in-wheel motors. As mentioned previously, the 4IDEV is an over-actuated system, so the multi-objective control method can be employed to enhance the system performance in different aspects. In this section, a multi-objective optimal torque distribution strategy is proposed to improve the total energy efficiency of vehicle while tracking the desired yaw moment calculated by the yaw stability controller. The controller is designed based on hMPC and the nonlinear characteristic of motor energy loss function is considered.

A. DYNAMIC MODEL IN TORQUE DITRIBUTION PROBLEM

The proposed dynamic model consists of a four wheel vehicle dynamic model and a piecewise linear approximation of energy loss function.

1) FOUR WHEEL VEHICLE DYNAMIC MODEL

A four wheel vehicle dynamic model is formulated to determine the optimal driving torques or braking torques of motors. The schematic diagram of a 4IDEV is shown in Fig. 9, which neglects the vertical motion and the lateral force difference between two sides.

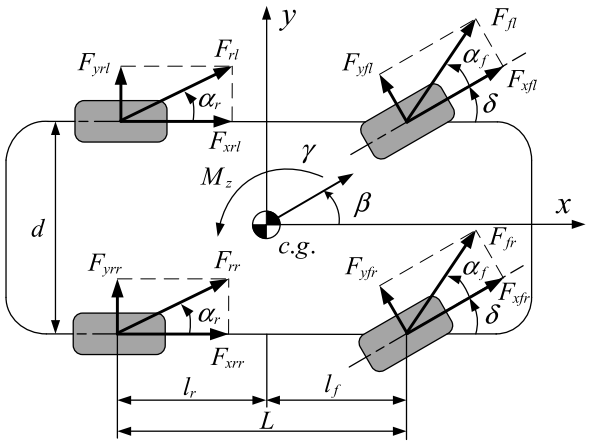

FIGURE 9. Four wheel vehicle dynamic model.

According to (15) and (16), the yaw moment generated by lateral forces has already been expressed by a function of α_f and α_r. Hence, the reference yaw moment M_z is generated by longitudinal forces. The total longitudinal force F_x and the reference yaw moment M_z is expressed in

$$\begin{aligned} F_x &= F_{xfr} + F_{xfl} + F_{xrr} + F_{xrl} \\ M_z &= \frac{d}{2}(-F_{xfr}\cos\delta + F_{xfl}\cos\delta - F_{xrr} + F_{xrl}) \\ &\quad + l_f F_{xfr}\sin\delta + l_f F_{xfl}\sin\delta \end{aligned} \tag{29}$$

where $F_{xfr}, F_{xfr}, F_{xfr}, F_{xfr}$ are longitudinal forces, d is wheelbase and δ is steering angle. Since the steering angle δ is normally small, (29) can be simplified as follows:

$$\begin{aligned} F_x &= F_{xfr} + F_{xfl} + F_{xrr} + F_{xrl} \\ M_z &= \frac{d}{2}(-F_{xfr} + F_{xfl} - F_{xrr} + F_{xrl}) \end{aligned} \tag{30}$$

The longitudinal forces can be approximated as follows [12], [13]:

$$F_{xij} = \frac{T_{ij}\cdot i_0}{r} \tag{31}$$

where T represents the motor torque. Hence, (30) can be rewritten as follows:

$$\begin{aligned} F_x &= ri_0(T_{fr} + T_{fl} + T_{rr} + T_{rl}) \\ M_z &= \frac{dri_0}{2}(-T_{fr} + T_{fl} - T_{rr} + T_{rl}) \end{aligned} \tag{32}$$

2) PIECEWISE LINEAR ENERGY LOSS MODEL

According to previous discussion, the motor power loss function varies with torque and motor speed and the motor speed can be obtained by the vehicle velocity v_x. And $P_L(T)$ can be further determined. Hence, the piecewise linear approximation is obtained for the multi-objective torque distribution controller. The piecewise linear function approximation of $P_L(T)$ is expressed in

$$P_L(T) = \begin{cases} k_1 T & \text{if } T \in [0, T_1) \\ k_2 T + m_1 & \text{if } T \in [T_1, T_2) \\ k_3 T + m_2 & \text{if } T \in [T_2, T_3) \\ k_4 T + m_3 & \text{if } T \in [T_3, T_4) \\ k_5 T + m_4 & \text{if } T \in [T_4, 90] \end{cases} \tag{33}$$

where k_i and m_i are the fitting coefficients, T_i is the segregating point.

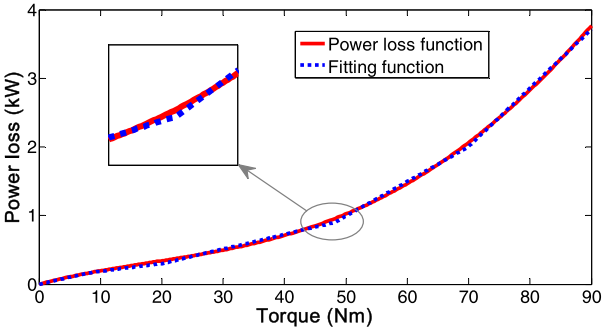

FIGURE 10. Motor power loss function at v_x=15 m/s.

As shown in Fig. 10, $P_L(T)$ is divided into five discrete regions, and the regions are switched by the segregating points. Fig. 10 illustrates that the fitting error between the piecewise linear curve and motor power loss function is quite small.

Hence, the total power loss of the 4IDEV is expressed in

$$\sum P_L = P_L(T_{fl}) + P_L(T_{fr}) + P_L(T_{rl}) + P_L(T_{rr}) \tag{34}$$

where $P_L(T_{ij})$ is the piecewise linear function shown in (33) and varies with the motor torque T_{ij} on each wheel.

B. MULTI-OBJECTIVE TORQUE DISTRIBUTION CONTROLLER DESIGN

1) PREDICTIVE MODEL FORMULATION

A predictive model of the multi-objective torque distribution controller is proposed in this section. The dynamic model can be formulated as the following:

$$\begin{aligned} \sum P_L &= P_L(T_{fl}) + P_L(T_{fr}) + P_L(T_{rl}) + P_L(T_{rr}) \\ M_z &= \frac{dri_0}{2}(-T_{fr} + T_{fl} - T_{rr} + T_{rl}) \end{aligned} \tag{35}$$

By substituting (33) into (35), the given equations can be rewritten as following matrix form:

$$\begin{aligned} \boldsymbol{\omega} &= \boldsymbol{B}_{pqmn}\boldsymbol{\xi} \\ \text{if } \sum P_L &\in P_{Lpqmn} \end{aligned} \tag{36}$$

where $\boldsymbol{\omega} = [\sum P_L M_z]^T$, $\boldsymbol{\xi} = [T_{fl}T_{fr}T_{rl}T_{rr}]^T$. The matrix $\boldsymbol{B}_{pqmn}$, $p, q, m, n \in \{1, \ldots, 5\}$ is determined by discrete regions of $P_L(T_{ij})$.

Same as the design process of yaw stability controller, (36) is formulated to an extended closed-loop discrete-time system by defining E_s as the accumulative tracking error of M_z. Thereby, the predictive model is expressed in

$$\begin{aligned} \boldsymbol{\omega_{e(k+1)}} &= \boldsymbol{B}^*_{pqmn}\boldsymbol{\xi}_{(k)} \\ \text{if} \sum P_{L(k)} &\in P_{Lpqmn} \end{aligned} \tag{37}$$

where $\boldsymbol{\omega}_e = [\sum P_L M_z E_s]^T$, $\boldsymbol{B}^*_{pqmn}$ is the discretized corresponding matrix.

For the further application in the multi-objective controller, (37) is transformed to a MLD model by using the HYSDEL. The MLD model in torque distribution problem can be expressed as follows:

$$\begin{aligned} \boldsymbol{\omega}_{e(k\mathcal{C}1)} &= \boldsymbol{B}^*\boldsymbol{\xi}_{(k)} + \boldsymbol{B}^*_1\boldsymbol{v}^*_{(k)} + \boldsymbol{B}^*_2\boldsymbol{z}^*_{(k)}\boldsymbol{E}^*_1\boldsymbol{v}^*_{(k)} + \boldsymbol{E}^*_2\boldsymbol{z}^*_{(k)} \\ &\le \boldsymbol{E}^*_3\boldsymbol{\omega}_{e(k)} + \boldsymbol{E}^*_4\boldsymbol{\xi}_{(k)} + \boldsymbol{E}^*_5 \end{aligned} \tag{38}$$

where $\boldsymbol{v}^*_{(k)}, \boldsymbol{z}^*_{(k)}$ are the auxiliary binary and continuous variables, and $\boldsymbol{B}^*, \boldsymbol{B}^*_1, \boldsymbol{B}^*_2, \boldsymbol{E}^*_1, \ldots, \boldsymbol{E}^*_5\boldsymbol{E}_5$ are matrices of suitable dimensions determined by HYSDEL.

2) REFERENCE AND CONSTRAINTS

The reference of yaw moment is calculated in real time by the proposed yaw rate controller and the reference of total power loss is set to zero.

Moreover, constrains of motor torques can be determined by the maximum motor torque $T_{\max}$ and the longitudinal driving resistance F_r. The constrain of motor torque is described as follows:

$$0 \le T_{ij} \le T_{\max} \sum T_{ij} = \frac{F_x}{ri_0} = \frac{F_r}{ri_0} \tag{39}$$

3) OPTIMIZATION OBJECTIVE

The cost function of the proposed multi-objective torque distribution controller is defined as the sum of the 2-norm case of the matrix which reflects the distance between the states and reference values. Hence, the objective of the controller consists of two parts, i.e., minimize the tracking error of yaw moment and total energy consumption of the vehicle. According to the hMPC algorithm, the whole control problem can be divided into receding horizon control problems. The control problem to minimize the cost function at the k-th sampling time is shown as follows:

$$\begin{aligned} &\min J_k = \min_{k \to k+N-1} \|\boldsymbol{\Omega_k} - \boldsymbol{R_k}\|^2_{\boldsymbol{Q}} \\ &= \min \sum_{i=0}^{N-1} (\omega_{k+i|k} - r_{k+i|k})^T \boldsymbol{Q}(\omega_{k+i|k} - r_{k+i|k}) \\ &\text{subj.to.} \\ &\quad \boldsymbol{\omega_{e(k+1)}} = \boldsymbol{B}^*\boldsymbol{\xi}_{(k)} + \boldsymbol{B}^*_1\boldsymbol{v}^*_{(k)} + \boldsymbol{B}^*_2\boldsymbol{z}^*_{(k)} \\ &\quad \boldsymbol{E}^*_1\boldsymbol{v}^*_{(k)} + \boldsymbol{E}^*_2\boldsymbol{z}^*_{(k)} \le \boldsymbol{E}^*_3\boldsymbol{\omega}_{e(k)} + \boldsymbol{E}^*_4\boldsymbol{\xi}_{(k)} + \boldsymbol{E}^*_5 \\ &\quad \xi_{(k+i|k)} \in \boldsymbol{\Xi_k}, \boldsymbol{\omega}_{e(k|k)} = \boldsymbol{\omega}_{e(k)}, \boldsymbol{\omega}_{e(k+N|k)} \in \boldsymbol{\chi}_f \\ &\quad 0 \le T_{ij} \le T_{\max} \\ &\quad \sum T_{ij} = \frac{F_x}{ri_0} = \frac{F_r}{ri_0} \end{aligned} \tag{40}$$

where $\boldsymbol{\Xi_k} = \begin{bmatrix} \xi_{k|k} \\ \xi_{k+1|k} \\ \cdot \\ \cdot \\ \xi_{k+N-1|k} \end{bmatrix}_N \subseteq \mathbb{R}^N$, $\boldsymbol{\Omega_k} = \begin{bmatrix} \omega_{k|k} \\ \omega_{k+1|k} \\ \cdot \\ \cdot \\ \omega_{k+P-1|k} \end{bmatrix}_P \in \mathbb{R}^P \in R^P$ and $\boldsymbol{R_k} = \begin{bmatrix} r_{k|k} \\ r_{k+1|k} \\ \cdot \\ r_{k+N-1|k} \end{bmatrix}_P \in \mathbb{R}^P$ are the control sequence, output sequence and output reference sequence, respectively. $\boldsymbol{\omega_{e(k)}}$ is the state at the k-th sampling time, $\boldsymbol{\chi}_f$ is the controller terminal set. $\boldsymbol{Q}$ is the weight matrix.

Considering the logical variables in the constraints defined in the MLD model, the receding horizon control problem shown in (40) comes down to solve a MIQP problem.

V. SIMULATION RESULTS AND DISCUSSION

In this section, the performance of suggested yaw stability controller and torque distribution strategy is evaluated on the dSPACE-based platform, as shown in Fig. 11. The proposed strategy is run on the dSPACE autobox with the signals from the vehicle control unit (VCU). The real-time online simulation in this section is in process via the dSPACE Midsize Simulator. Considering the overall evaluation and performance verification of the control strategy, the simulation is carried out with two vehicle maneuvers: single lane change test and fishhook steering test. The parameters of 4IDEV are presented in Table 3. In the proposed hMPC controller, the sampling time, the control horizon N and prediction horizon P are set to $T_s = 5\text{ms}, N = P = 3$, respectively.

A. SINGLE LANE CHANGE TEST

To analyze the effectiveness of the proposed yaw stability controller and torque distribution strategy, a single lane

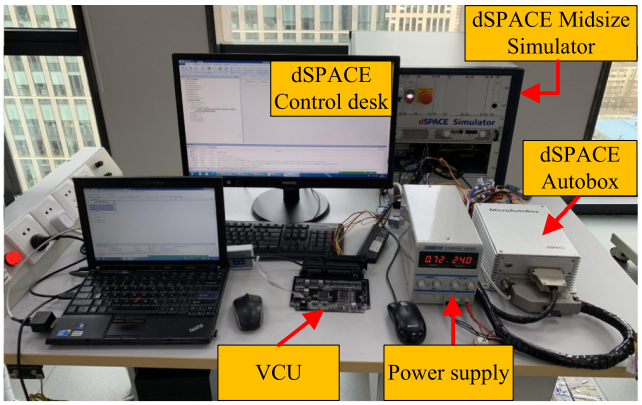

FIGURE 11. DSPACE-based test platform.

TABLE 3. Main parameters of 4IDEV.

Para	Value	Unit	Para	Value	Unit
v_x	54	km/h	r	0.354	m
m	1523	kg	A_s	1.95	m^2
l_f	1.163	m	l_r	1.385	m
c_f	130434	N/rad	c_r	105154	N/rad
I_z	2023	kg·m^2	i_0	7.1	-
d	1.539	m			

change test is conducted firstly. As one of the most commonly used test maneuvers for vehicle handling stability evaluation, the single lane change test generally takes a sinusoidal steering angle as the input. As shown by the blue dotted line in Fig. 12(a), the front wheel steering angle δ is set to a sine wave with a period of 2 seconds and an amplitude of 5 degrees when the 4IDEV runs at a constant longitudinal velocity $v_x = 15$ m/s on a high friction-coefficient road. The simulation results are given in Fig. 12(a)-(g).

The performance of the hMPC controller to stabilize the vehicle is shown first in Fig. 12(a). Since the sinusoidal steering is applied at $t = 1.5$ s, the yaw rate of vehicle rapidly increases and the vehicle even tends to spin at $t = 3$ s when there is no any active control working. Nevertheless, once the hMPC-based vehicle yaw stability controller is applied on the vehicle, the value of the yaw rate is stabilized. Meanwhile, the tracking error between the optimal yaw rate and reference value approaches zero. According to the comparison results in Fig. 12(a), it's obvious that the yaw stability controller can stabilize the vehicle effectively and track the desired yaw rate quickly and precisely.

Fig. 12(b) shows the optimal control variables in the hMPC controller, i.e., the active steering angle and the yaw moment generated by the differential driving between four motors. Compared to the steering angle from the driver in Fig. 12(a), the optimal steering angle has a similar value. Considering the improvement of yaw stability shown in Fig. 12(a), the control of the active yaw moment has a marked effect. Furthermore, the absolute value of the yaw moment is strictly restricted with an upper limit value based on the motor driving capability.

Fig. 12(c) shows the tire sideslip angles comparison between hMPC control and that without control. The tire sideslip angles are extremely large and a non-convergence issue arises when the yaw stability controller is inoperative. Once the hMPC controller working, the values of these states reduce rapidly and more states reach the stable region, which means the stability of the 4IDEV is enhanced. It is worth noting that there is state region switching of the tire sideslip angle over the simulation time, which reflects the practicability of the hMPC controller in hybrid system.

Fig. 12(d) illustrates the yaw moment tracking results of different control methods. The ESC means only the yaw stability is considered during the torque distribution process, and the multi-objective control takes both of the yaw stability and energy consumption of the 4IDEV into account. Despite there is a certain lag, both of the above two control methods can track the optimized yaw moment well. In addition, the value of the yaw moment in the torque distribution strategy does not exceed the limit.

Fig. 12(e) and Fig. 12(f) show the torque distribution results in the ESC and the multi-objective control. FL, FR,

RL, RR mean the front-left, front-right, rear-left and rear-right motors, respectively. In Fig. 12(e), when there is no steering, the torque of each wheel retains invariant and even. However, the multi-objective control can redistribute the torques of four motors to minimize the power loss while meeting the requisite driving torque compared to the ESC method, as shown in Fig. 12(f). When the lateral dynamics of 4IDEV become unstable at $t = 1.5$ s, the torques of four motors change and the variation trend of the two motors on one axle is opposite. Accordingly, the required yaw moment in the single lane change maneuver can be generated by the driving or braking torques of four in-wheel motors, as well as the requisite driving torque. In Fig. 12(e), the torques of four motors distributed based on the yaw stability control jump up and down frequently, which is caused by the multiple solutions when the control objective only consists of the vehicle yaw stability. This phenomenon has improved a lot when the energy consumption is taken into consideration, as shown in Fig. 12(f).

Fig. 12(g) depicts the total power loss of four motors in the cases of under ESC and multi-objective control. As can be seen from the simulation results in Table 4, compared to the ESC method, the suggested multi-objective torque distribution strategy can reduce the power loss of the drivetrain by 26.7% during the entire simulation. It is noteworthy that the simple even torque distribution strategy loses more electric energy than the multi-objective control strategy when the 4IDEV goes straight at the first 1.5 s. When the vehicle runs in the single lane change maneuver at $t = 1.5 - 3.5$ s, the suggested strategy can further allocate the motor torque under the premise of satisfying the yaw stability, the decline of power loss is up to 20.1%. Therefore, the multi-objective

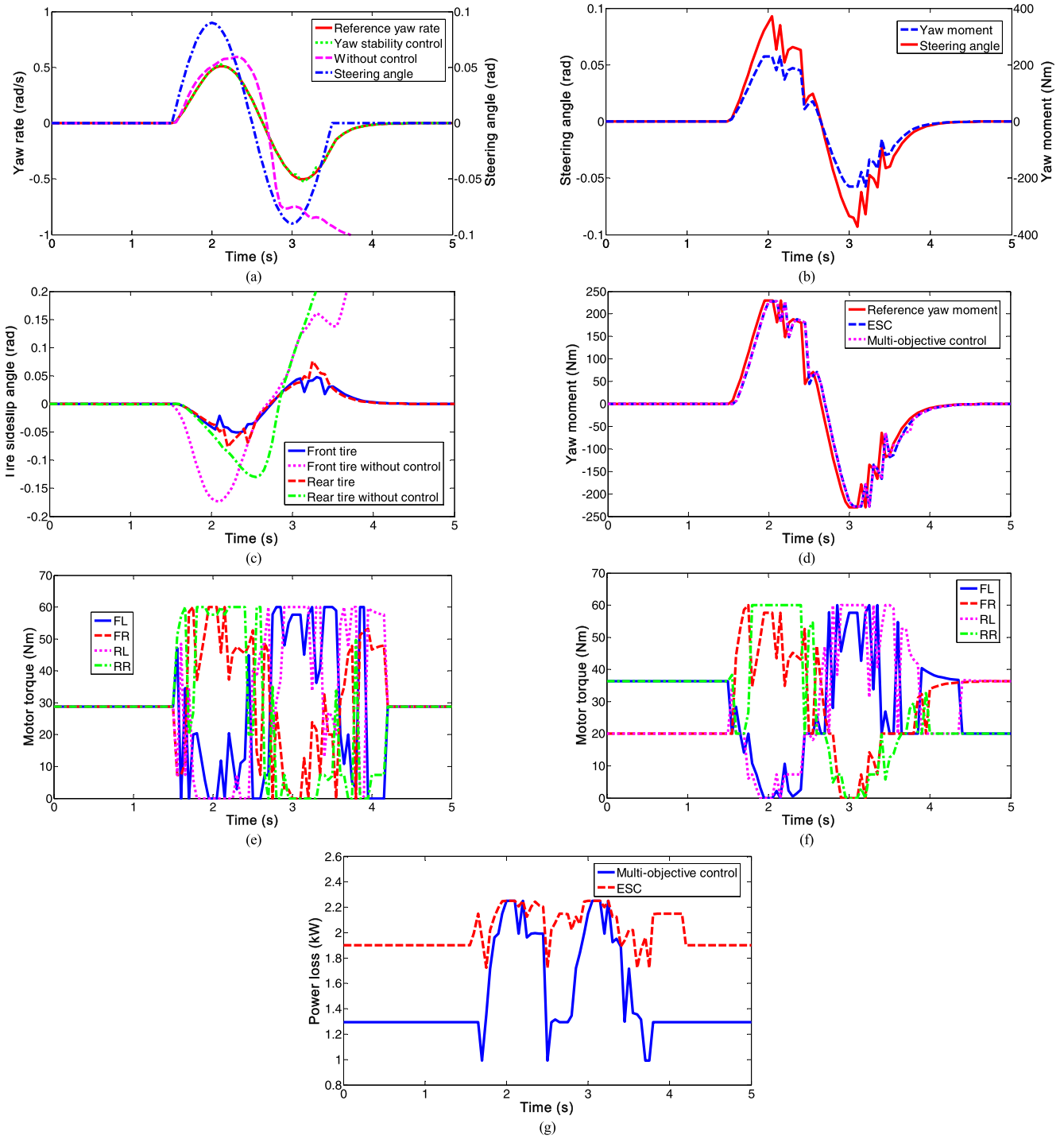

FIGURE 12. Simulation results of the single lane change test. (a) steering angle and yaw rate. (b) optimal steering angle and yaw moment. (c) front and rear tires sideslip angle. (d) yaw moment tracking. (e) torques of four motor under ESC. (f) torques of four motor under multi-objective control. (g) total power loss of four motors.

torque distribution strategy is fruitful in reducing the power loss of the drivetrain.

B. FISHHOOK STEERING TEST

To further illustrate the control performance of the suggested method, a fishhook steering test is conducted at a constant longitudinal velocity $v_x = 15$ m/s. The fishhook maneuver is to simulate the driver behavior when avoiding obstacles on the road. The simulation results are given in Fig. 13(a)-(g).

Fig. 13(a) shows the steering angle in fishhook maneuver, the reference yaw rate and yaw rate without control and with yaw stability control, respectively. When there is no

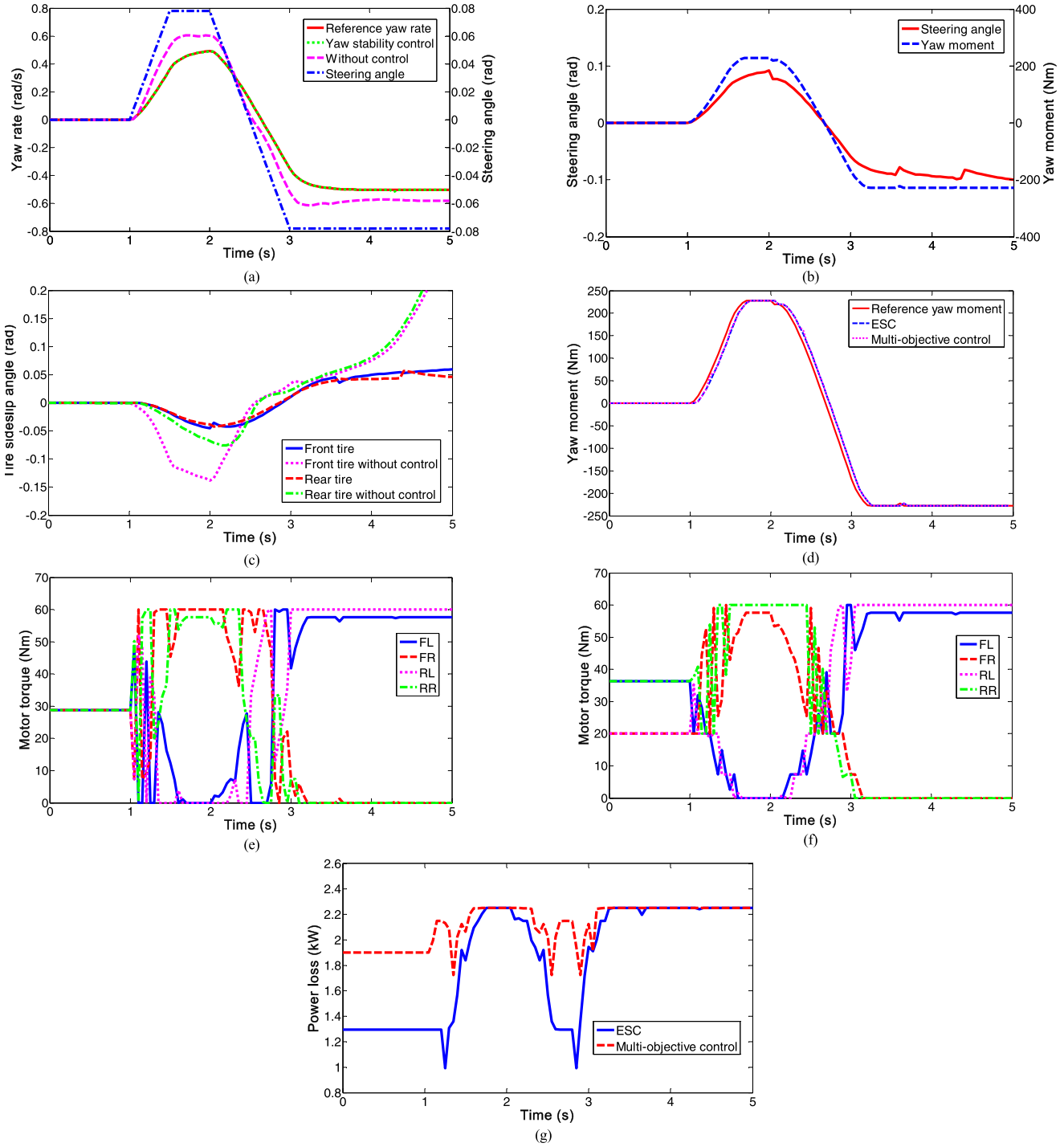

FIGURE 13. Simulation results of the fishhook steering test. (a) steering angle and yaw rate. (b) optimal steering angle and yaw moment. (c) front and rear tires sideslip angle. (d) yaw moment tracking. (e) four motor torque under ESC. (f) four motor torque under multi-objective control. (g) total power loss of four motors.

control applied on the vehicle, the yaw rate deviates from the reference signal with a 0.1 rad/s tracking error. In contrast, the above-mentioned phenomenon will ameliorate a lot when the hMPC controller takes effect. Hence, the yaw stability controller is capable of enhancing the handling performance and safety of the 4IDEV in the fishhook maneuver.

Fig. 13(b) and Fig. 13(c) show the varying curves of the optimal control variables and states in the hMPC controller. In Fig. 13(b), the value of the yaw moment is limited due to the constraints defined in previous sections. Even so, the better performance of the stability is achieved as shown in Fig. 13(c). Compared to the non-control results, the tire

TABLE 4. Power loss comparison.

Distribution strategy	Single line change(kW)		Fishhook steering(kW)	
	Total	Steering	Total	Steering
ESC	203.5	88.7	214.9	175.9
Multi-objective	149.1	70.9	185.6	161.1
Improvements	26.7%	20.1%	13.6%	8.3%

sideslip angles under the proposed control method are in the stable region basically. Fig. 13(d) illustrates the comparison of yaw moment tracking between the ESC method and multi-objective control method. Both strategies are expert at tracking the reference yaw moment and the tracking performance is almost the same in this maneuver.

The torque distribution results of four motors are shown in Fig. 13(e) and Fig. 13(f) based on the reference yaw moment in Fig. (d). Considering the power loss of drivetrain, torques in the first 1.5 s are redistributed with the multi-objective control instead of the even distribution strategy. In addition, the motor torques have lower varying frequency compared to the ESC method. Besides, as shown in Fig. 13(g), it is obvious that the power loss of drivetrain is significantly reduced. As shown in Table 3, the declines of the power loss during the fishhook steering maneuver ($t = 1.5 - 3.5$ s) and entire simulation cycle reach 8.4% and 13.6%, respectively. Therefore, the multi-objective torque distribution strategy can reduce vehicle energy consumption while ensuring the yaw stability.

VI. CONCLUSION

The presented study in this paper proposes a novel multi-objective optimal torque distribution strategy considering vehicle stability and energy consumption for the 4IDEV. First, the energy loss model is built to describe the motor efficiency characteristics properly. An EECA strategy is proposed based on the energy loss model and reduces the total power loss by 9.29% over the NEDC. Then, a piecewise linear vehicle dynamic model is presented considering the nonlinear characteristics of tires. On the basis of the hMPC algorithm, a yaw stability controller is designed to enhance the handling performance and safety of 4IDEV by forcing the yaw rate to track the desired value quickly and precisely. Based on this argument, the multi-objective torque distribution strategy is developed to allocate the driving torques or braking torques of four in-wheel motors. Finally, the effectiveness of the suggested method was verified in the dSPACE Midsize Simulator. Compared to the ESC method, the proposed multi-objective optimal torque distribution strategy can reduce the power loss of the drivetrain by 26.7% and 13.6% in the single lane change test and fishhook steering test while ensuring the yaw stability.

REFERENCES

[1] Y. Hori, "Future vehicle driven by electricity and control-research on four-wheel-motored 'UOT electric march II'," *IEEE Trans. Ind. Electron.*, vol. 51, no. 5, pp. 954–962, Oct. 2004.

[2] S. Sakai, H. Sado, and Y. Hori, "Motion control in an electric vehicle with four independently driven in-wheel motors," *IEEE/ASME Trans. Mechatronics*, vol. 4, no. 1, pp. 9–16, Mar. 1999.

[3] Y. Chen and J. Wang, "Design and evaluation on electric differentials for overactuated electric ground vehicles with four independent in-wheel motors," *IEEE Trans. Veh. Technol.*, vol. 61, no. 4, pp. 1534–1542, May 2012.

[4] D. Zhang, G. Liu, H. Zhou, and W. Zhao, "Adaptive sliding mode fault-tolerant coordination control for four-wheel independently driven electric vehicles," *IEEE Trans. Ind. Electron.*, vol. 65, no. 11, pp. 9090–9100, Nov. 2018.

[5] J. Brembeck and P. Ritzer, "Energy optimal control of an over actuated robotic electric vehicle using enhanced control allocation approaches," in *Proc. IEEE Intell. Vehicles Symp.*, Alcalá de Henares, Spain, Jun. 2012, pp. 322–327.

[6] H. Zhou, F. Jia, H. Jing, Z. Liu, and L. Güvenç, "Coordinated longitudinal and lateral motion control for four wheel independent motor-drive electric vehicle," *IEEE Trans. Veh. Technol.*, vol. 67, no. 5, pp. 3782–3790, May 2018.

[7] S. Sakai, H. Sado, and Y. Hori, "Dynamic driving/braking force distribution in electric vehicles with independently driven four wheels," *Elect. Eng. Jpn.*, vol. 138, no. 1, pp. 79–89, Jan. 2002.

[8] P. Falcone, F. Borrelli, J. Asgari, H. E. Tseng, and D. Hrovat, "Predictive active steering control for autonomous vehicle systems," *IEEE Trans. Control Syst. Technol.*, vol. 15, no. 3, pp. 566–580, May 2007.

[9] B.-C. Chen and C.-C. Kuo, "Electronic stability control for electric vehicle with four in-wheel motors," *Int. J. Automot. Technol.*, vol. 15, no. 4, pp. 573–580, 2014.

[10] M. Choi and S. B. Choi, "Model predictive control for vehicle yaw stability with practical concerns," *IEEE Trans. Veh. Technol.*, vol. 63, no. 8, pp. 3539–3548, Oct. 2014.

[11] L. De Novellis, A. Sorniotti, and P. Gruber, "Wheel torque distribution criteria for electric vehicles with torque-vectoring differentials," *IEEE Trans. Veh. Technol.*, vol. 63, no. 4, pp. 1593–1602, May 2014.

[12] L. Zhai, T. Sun, and J. Wang, "Electronic stability control based on motor driving and braking torque distribution for a four in-wheel motor drive electric vehicle," *IEEE Trans. Veh. Technol.*, vol. 65, no. 6, pp. 4726–4739, Jun. 2016.

[13] M. Liu, J. Huang, and M. Cao, "Handling stability improvement for a four-axle hybrid electric ground vehicle driven by in-wheel motors," *IEEE Access*, vol. 6, pp. 2668–2682, 2018.

[14] K. Nam, S. Oh, H. Fujimoto, and Y. Hori, "Robust yaw stability control for electric vehicles based on active front steering control through a steer-by-wire system," *Int. J. Automot. Technol.*, vol. 13, no. 7, pp. 1169–1176, 2012.

[15] W. Zhao, X. Qin, and C. Wang, "Yaw and lateral stability control for four-wheel steer-by-wire system," *IEEE/ASME Trans. Mechatronics*, vol. 23, no. 6, pp. 2628–2637, Dec. 2018.

[16] S. Di Cairano, H. E. Tseng, D. Bernardini, and A. Bemporad, "Vehicle yaw stability control by coordinated active front steering and differential braking in the tire sideslip angles domain," *IEEE Trans. Control Syst. Technol.*, vol. 21, no. 4, pp. 1236–1248, Jul. 2013.

[17] H. Zhao, B. Gao, B. Ren, and H. Chen, "Integrated control of in-wheel motor electric vehicles using a triple-step nonlinear method," *J. Franklin Inst.*, vol. 352, no. 2, pp. 519–540, 2015.

[18] B. Ren, H. Chen, H. Zhao, and L. Yuan, "MPC-based yaw stability control in in-wheel-motored EV via active front steering and motor torque distribution," *Mechatronics*, vol. 38, pp. 103–114, Sep. 2016.

[19] X. Xie, L. Jin, Y. Jiang, and B. Guo, "Integrated dynamics control system with ESC and RAS for a distributed electric vehicle," *IEEE Access*, vol. 6, pp. 18694–18704, 2018.

[20] J. Guo, Y. Luo, and K. Li, "An adaptive hierarchical trajectory following control approach of autonomous four-wheel independent drive electric vehicles," *IEEE Trans. Intell. Transp. Syst.*, vol. 19, no. 8, pp. 2482–2492, Aug. 2018.

[21] Y. Chen and J. Wang, "Fast and global optimal energy-efficient control allocation with applications to over-actuated electric ground vehicles," *IEEE Trans. Control Syst. Technol.*, vol. 20, no. 5, pp. 1202–1211, Sep. 2011.

[22] Y. Chen and J. Wang, "Design and experimental evaluations on energy efficient control allocation methods for overactuated electric vehicles: Longitudinal motion case," *IEEE/ASME Trans. Mechatronics*, vol. 19, no. 2, pp. 538–548, Apr. 2014.
[23] X. Yuan and J. Wang, "Torque distribution strategy for a front- and rear-wheel-driven electric vehicle," *IEEE Trans. Veh. Technol.*, vol. 61, no. 8, pp. 3365–3374, Oct. 2012.
[24] A. M. Dizqah, B. Lenzo, A. Sorniotti, P. Gruber, S. Fallah, and J. De Smet, "A fast and parametric torque distribution strategy for four-wheel-drive energy-efficient electric vehicles," *IEEE Trans. Ind. Electron.*, vol. 63, no. 7, pp. 4367–4376, Jul. 2016.
[25] Z. Wang, C. Qu, L. Zhang, X. Xue, and J. Wu, "Optimal component sizing of a four-wheel independently-actuated electric vehicle with a real-time torque distribution strategy," *IEEE Access*, vol. 6, pp. 49523–49536, 2018. doi: 10.1109/ACCESS.2018.2801564.
[26] R. He, Z. Song, J. Li, and M. Ouyang, "Optimal torque distribution strategy considering energy loss and tire adhesion for 4WD electric vehicles," in *Proc. IEEE Transp. Electrific. Conf. Expo, Asia–Pacific*, Harbin, China, Aug. 2017, pp. 1–6.
[27] C. Lin and Z. Xu, "Wheel torque distribution of four-wheel-drive electric vehicles based on multi-objective optimization," *Energies*, vol. 8, no. 5, pp. 3815–3831, 2015.
[28] H. Jing, F. Jia, and Z. Liu, "Multi-objective optimal control allocation for an over-actuated electric vehicle," *IEEE Access*, vol. 6, pp. 4824–4833, 2018.
[29] J. Chen, C. Lin, and S. Liang, "Mixed logical dynamical model-based MPC for yaw stability control of distributed drive electric vehicles," presented at the 10th Int. Conf. Appl. Energy, Hong Kong, Aug. 2018.
[30] A. Bemporad and M. Morari, "Control of systems integrating logic, dynamics, and constraints," *Automatica*, vol. 35, no. 3, pp. 407–427, Mar. 1999.
[31] F. D. Torrisi and A. Bemporad, "HYSDEL-a tool for generating computational hybrid models for analysis and synthesis problems," *IEEE Trans. Control Syst. Technol.*, vol. 12, no. 2, pp. 235–249, Mar. 2004.
[32] J. B. Rawlings, D. Q. Mayne, *Model Predictive Control Theory and Design*. Madison, WI, USA: Nob Hill, 2009.

CHENG LIN received the B.S. and M.S. degrees in mechanical engineering from the Wuhan Institute of Technology, Wuhan, China, in 1990 and 1995, respectively, and the Ph.D. degree in mechanical engineering from the Beijing Institute of Technology, Beijing, China, in 2002.

Since 1995, he has been a Lecturer with the Department of Vehicle Engineering, School of Mechanical Engineering, Beijing Institute of Technology. In 2001, he was an Associate Professor with the Department of Vehicle Engineering, School of Mechanical Engineering, Beijing Institute of Technology. From 2010 to 2011, he was a Senior Research Fellow sponsored by the Country China Scholarship Council, Michigan University, Ann Arbor, MI, USA. He is currently a Professor, a Ph.D. Tutor, and the Deputy Director of the National Engineering Laboratory for Electric Vehicle, the Director of the Research Center for Electric Vehicle in Beijing, and an Academic Leader of the Collaborative Innovation Center of Electric Vehicles in Beijing. He was selected into the National High-Level Personnel of Special Support Program, in 2016. He has authored or coauthored more than 100 papers. He holds 126 patents. His current research interests include electric vehicle, vehicle dynamics, and the optimization and lightweight of automotive body structure.

Dr. Lin was a recipient of the Second Prize of the National Science and Technology Progress Award, in 2008, and the First Prize and the Second Prize of the Beijing Municipal Science and Technology Award, in 2010 and 2013, respectively.

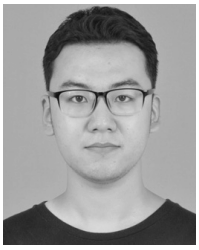

SHENG LIANG received the B.S. degree in vehicle engineering from the Beijing Institute of Technology, Beijing, China, in 2017, where he is currently pursuing the Ph.D. degree in mechanical engineering.

His current research interests include vehicle dynamics modeling and the multiobjective control algorithm for four in-wheel-motor drive electric vehicles.

JIAN CHEN received the B.S. degree in vehicle engineering from the Beijing Institute of Technology, Beijing, China, in 2017, where he is currently pursuing the M.S. degree in mechanical engineering.

His current research interests include nonlinear control algorithm, and the vehicle dynamics modeling and control for four in-wheel-motor drive electric vehicles.

XIANG GAO received the B.S. degree in vehicle engineering from Hunan University, in 2017. He is currently pursuing the M.S. degree in mechanical engineering with the Beijing Institute of Technology, Beijing, China.

His current research interests include energy management, and the vehicle dynamic modeling and torque distribution for four in-wheel-motor drive electric vehicles.